AMD Mapping in the Lusatian Region: From Medium to Very High-Resolution R/S Data

Delira Hanelli[a], Enis Sterjo[b], Roberto De La Rosa[c] and Andreas Knobloch[d]
Beak Consultants GmbH, Am St.-Niclas-Schacht 13, 09599 Freiberg, Germany

Keywords: Acid Mine Drainage, Lusatia, Artificial Neural Networks, Remote Sensing, Multispectral Imagery.

Abstract: The Lusatian region is undergoing an extensive landscape rehabilitation program following the closure of lignite open-pit mines. Under this programme, former open-cast lignite mines are being converted into artificial water bodies. However, the region faces significant challenges related to the acidification of surface and groundwater primarily driven by the oxidation of pyrite. Recent geochemical analyses show that, surface waters exhibit a strong variation of pH and iron concentration. This study aims to elaborate the potential of free and commercial space- and airborne- multispectral Remote Sensing (R/S) datasets (Sentinel-2, Worldview-3 and Unmanned Aerial Vehicle (UAV)) for large-scale acid mine drainage (AMD) mapping and identify the most suitable data sources and approaches for practical case studies. Additionally, cross-sensor comparisons are performed to gain more insights into the agreement between the spectra from Sentinel-2 images with those from the Worldview-3 and UAV images over surface water. The cross-sensor agreement of the images is quantified by performing regression analyses between R/S data at different wavelengths. Finally, dependencies and relationships between AMD constituents and the spectral data are investigated using artificial neural networks (ANN) of type Multi-Layer Perceptron (MLP).

1 INTRODUCTION

The Lusatian region in Germany, well-known for lignite mining, is currently undergoing one of the largest landscape rehabilitation programs in Europe (LMBV, n.d.). Following the closure of open-pit lignite mines, the region comprises approximately 176 artificial water bodies, covering a total area of 185 km² (Hanelli, et al., 2023). Leading this large-scale transformation and rehabilitation, the Lausitzer und Mitteldeutsche Bergbau-Verwaltung (LMBV) is monitoring the water quality in these water bodies by periodic sampling campaigns and geochemical analyses.

The water quality across the region varies significantly due to differences in acid mine drainage (AMD) stages, water treatment methods, and geological conditions. For instance, newly flooded or untreated lakes often exhibit highly acidic conditions, with pH values between 2.5 and 4.5, whereas treated and naturally neutralized lakes typically range between 6.5 and 8 (LMBV, n.d.). Given its complexity and large spatial extent, the Lusatian region presents an ideal case study for developing and validating cost-effective AMD mapping methods.

Remote sensing (R/S) technologies offer promising solutions for large-scale AMD monitoring (Hanelli et al., 2023; Farahnakian et al., 2024; Kopačková, 2019). This study evaluates the potential of free and commercial multispectral datasets from spaceborne and airborne platforms for AMD mapping in a selected area of the Lusatian region characterized by strong AMD variations. A key focus is on cross-sensor comparisons to assess spectral data consistency across platforms and the transferability of AMD-related spectral relationships.

The multispectral R/S datasets utilized in this study include Sentinel-2, WorldView-3, and Unmanned Aerial Vehicle (UAV) data. These datasets cover different areas of interest (AOI) depending on their availability, costs and accessibility (Figure 1). The free-of-charge Sentinel-2 data cover

[a] https://orcid.org/0009-0002-0012-1729
[b] https://orcid.org/0009-0009-0993-0750
[c] https://orcid.org/0000-0002-3004-7104
[d] https://orcid.org/0000-0001-7515-001X

Hanelli, D., Sterjo, E., De La Rosa, R. and Knobloch, A.
AMD Mapping in the Lusatian Region: From Medium to Very High-Resolution R/S Data.
DOI: 10.5220/0013497200003935

In *Proceedings of the 11th International Conference on Geographical Information Systems Theory, Applications and Management (GISTAM 2025)*, pages 305-316
ISBN: 978-989-758-741-2; ISSN: 2184-500X

an extensive area of post-mining water bodies and several AMD scenarios. In contrast, the commercial WorldView-3 data were acquired only for a 100 km² representative area with significant AMD activity.

In most of the post-mining lakes in the Lusatian region the access is restricted due to geotechnical instabilities (ground subsidence and landslides) and very acidic water environments (LMBV, n.d.). Given these limitations and the objectives of this study, two pilot sites were selected for UAV surveys: Scheibe See (685 hectares, no evidence of AMD) and Bergheider See (325 hectares, evidence of AMD).

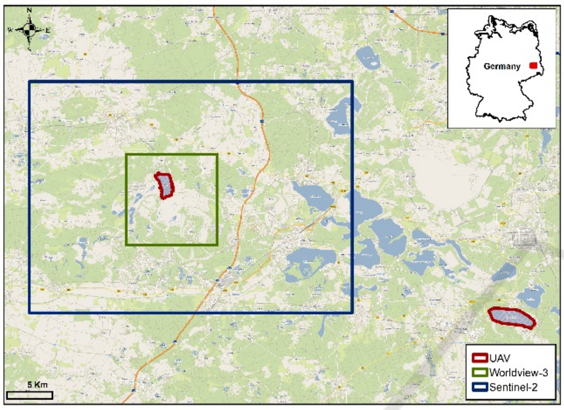

Figure 1: AOIs for each of the used R/S datasets.

The R/S datasets were utilised as key parameters for area-wide mapping of AMD in post-mining water bodies. At the same time, geochemical analyses of AMD components, such as iron concentration and pH values obtained from surface water samples, served as calibration data for the mapping process. The relationships between the AMD components and the spectral data are exploited by means of artificial neural networks (ANNs).

This application requires a synchronization of R/S datasets with geochemical analysis, in order to ensure that the measured water quality parameters correspond to the recorded surface reflectance information in the R/S datasets. This is particularly challenging considering the prerequisites of optical R/S imagery (e.g. cloud- and shadow-free, low-nadir-angle etc.). To increase the chances of getting suitable acquisitions, a temporal window of ± 10 – 20 days to the sampling date was applied, assuming no significant geochemical changes within this timeframe (e.g., through neutralization processes). This study integrates both R/S and geochemical datasets collected in late June 2024.

The study aims to improve AMD mapping techniques and identify the most effective and practical methodologies for environmental monitoring in post-mining landscapes.

2 DATA ACQUISITION

2.1 Geochemical Analysis

Geochemical analysis results for 31 post-mining water bodies were provided by LMBV for this study (Figure 2). The samples were collected from the epilimnion layer (0–15 m depth). Figure 1 shows the measured values of iron concentration as graduated symbols/colours, while the measured pH values are shown as column chart, whereas small columns indicate an acidic environment (pH varies between 2 and 3) and the big ones a neutral environment (pH varies between 6 and 8).

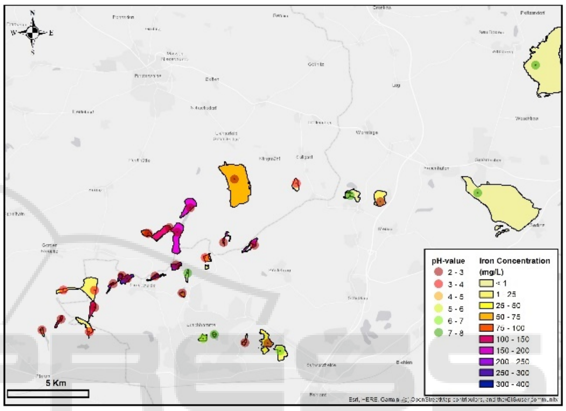

Figure 2: Water monitoring stations and recorded values of AMD constituents in the Lusatian post-mining water bodies.

The water bodies in this region are characterized by strongly varying AMD levels (Table 1) and are therefore suitable for this research study.

Table 1: Statistics of the water geochemical parameters.

Parameter	Count	Min	Max	Mean	Std
pH	31	2,45	7,96	3,77	1,90
Fe (mg/L)	31	0,07	361	90,65	101,42

Figure 3 shows a plot of dependencies between the iron concentration and pH values. Water bodies with high iron concentrations are typically marked by low pH values (≤4), while water bodies with low iron concentrations typically have pH values between 6 and 8. Although pH is an optically non-active parameter and cannot be directly detected using optical R/S data, in this study we use the observed dependencies for large-scale mapping of pH values by leveraging patterns of optically active constituents, such as iron concentration.

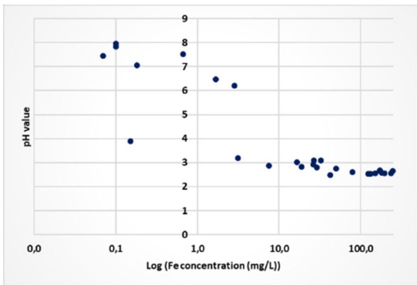

Figure 3: Plot of dependencies between Log (Fe) and pH.

2.2 R/S Datasets

An overview of the used R/S datasets for AMD mapping follows in Table 2. All data were projected to WGS1984/UTM 33N (WKID: 32633).

Table 2: Overview of the acquired imagery for AMD mapping (VNIR: visible and near-infrared, LWIR: Long-Wave Infrared, SWIR: Short-Wave Infrared).

Type	Sensor	Acquisition Date	Spectral Range	Temporal Res.	Spatial Res.	Cloud Cover	AOI
Space-Based Multispectral Imagery	Sentinel-2	16 June 2024	VNIR – SWIR 443–2190 nm	2 – 3 days Free of Charge	10, 20, 60 m	0.0[e]	Tile: T33UVT
Space-Based Super-spectral Imagery	Worldview-3	VNIR 26 June 2024 SWIR 29 June 2024	VNIR 400 - 1040 nm SWIR 1195 - 2365 nm	<1 day Commercial data	VNIR 1,24 m SWIR 3,70 m	0.0 0.0	100 km² surrounding Bergheider See
Airborne-Based Multispectral Imagery	DJI Matrice M300 RTK Micasense Altum-PT	10-25 June 2024	VNIR 475 to 842 nm LWIR 10500 nm	Commercial data	< 0,05 m	variable	Bergheider See and Scheibe See

2.2.1 Sentinel-2 Data

Sentinel-2 data were downloaded from https://code-de.org/de/. CODE-DE is part of Germany's geoinformation strategy and offers easy and efficient access to remote sensing data as well as free cloud resources for processing. More detailed information on the Sentinel-2 acquisition resolutions can be found on the Copernicus Sentinel-2 Mission website (Copernicus, n.d.).

For the AOI there is a wide archive of historical and actual data available. Top of Atmosphere (TOA) and Bottom of Atmosphere (BOA) products were downloaded respectively. The spatial resolution is set to 10 m to benefit from the medium spatial resolution of Sentinel-2 imagery.

[1] The cloud cover of Sentinel-2 acquisition over water bodies in the area of interest (AOI).

2.2.2 Worldview-3 Data

The commercial high-resolution (HR) Worldview-3 data (VNIR+SWIR) was ordered from European Space Imaging (https://www.euspaceimaging.com/) for a 100 km^2 representative area. More detailed information on the WorldView-3 data can be found on the ESA Earth Online website (European Space Agency [ESA], n.d.). Important prerequisites aspects to consider for optical analysis are the cloud coverage and the low nadir angle.

The data has been made available as Ortho-Ready Standard Product (OR2A), with the spectral data as Digital Numbers (DN). The DN values are further processed to TOA Reflectance values using the radiometric calibration tool supported by NV5 Geospatial's software tools (NV5 Geospatial, n.d.). The conversion to BOA reflectance resulted in negative reflectance values in water areas, because of the low radiance. It is important to highlight that the atmospheric corrections are designed for land applications, and not for water bodies. In water applications they modify the reflectance drastically. For this reason, TOA reflectance data are used for further processing.

2.2.3 UAV Data

The very-high resolution (VHR) UAV data were acquired from Beak Consultants GmbH with the following equipment:

- UAV: DJI Matrice M300 RTK,
- Multispectral camera: Micasense Altum-PT (detailed information can be found in the Altum-PT Integration Guide – MicaSense Knowledge Base [MicaSense, n.d.]),
- GPS/GNSS System: Emlid RS2 GPS/GNSS (Global Positioning System / Global Navigation Satellite System) with NTRIP (Networked Transport of RTCM via Internet Protocol) connection to the national CORS system (Continuously Operating Reference Station).

The necessary approvals/permissions for the UAV flights were obtained in advance based on the regulations of the German Federal Aviation Authority (LBA, n.d.).

The processing of UAV acquisitions relies on the Structure from motion (SfM) photogrammetric range imaging technique. However, applying this technique over large water bodies presents several challenges:

- High reflectivity: The reflective properties of water create a mirror-like effect.
- Dynamic surface conditions: The continuous movement of water, influenced by factors such as wind, introduces discrepancies of overlapping areas in consecutive scenes.
- Stereo image similarity: The homogeneity of stereo-image pairs over water surfaces makes it difficult to identify tie and key points necessary for accurate image alignment.

To align UAV acquisitions in this case study, we employed the image block-adjustment by reference technique, as implemented in Agisoft Metashape (Agisoft LLC, n.d.). This workflow includes a yaw estimation process that analyses the drone's flight path between consecutive images to determine the camera's horizontal rotation. Assuming zero pitch and roll, yaw is the only rotational parameter considered. The drone's movement direction is calculated by a direction vector, obtained by subtracting the current camera's location from the next camera's location. This process effectively determines the camera's horizontal orientation based on its movement relative to the previous shot, aiding in initial camera alignment for photogrammetric processing.

Because of the large areas, UAV flight campaigns are conducted over multiple days, often under varying illumination conditions, leading to variations in ground surface brightness. Figure 4 shows the tiles representing the flight missions and the weather conditions, respectively. To mitigate these variations, the sun sensor correction (DLS) is applied, which partially compensates for differences in lighting conditions during data acquisition. However, this approach assumes a constant irradiance over time and lacks to develop irradiance series and compensate the DLS for movement (MicaSense, n.d.).

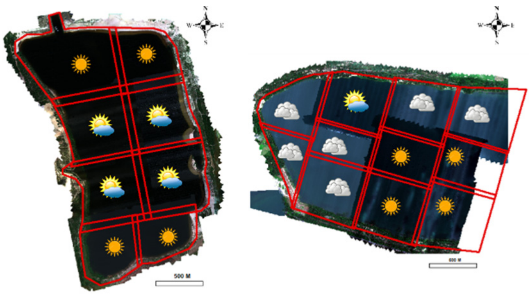

(a) (b)

Figure 4: The flight missions and respective weather conditions in a) Bergheider See and b) Scheibe See.

Finally, the recorded values have been divided by 32768 to get the reflectance values for each band instead of digital numbers (MicaSense, n.d.).

3 METHODS DESRCRIPTION

Dependencies and relationships between spectral reflectance bands and AMD constituents are investigated using the supervised machine learning (ML) algorithm of ANNs of the multilayer perceptron type (MLP) (Haykin, 1998). Additionally, cross-sensor comparisons (Chastain, et al., 2019) are performed to gain more insights into the agreement between the spectra from Sentinel-2 images with those from the Worldview-3 and UAV images over surface water. Finally, transformation parameters are calculated to harmonize Worldview-3 and UAV spectral bands to Sentinel-2 over water bodies.

3.1 Prediction Modelling Using Artificial Neural Networks

MLP ANNs are implemented in the advangeo® Prediction Software from Beak Consultants GmbH (www.advangeo.com). The modeling and prediction software analyses complex relationships between a wide variety of spatial influencing parameters (in this case the multispectral data) and given AMD occurrences, by using methods of artificial intelligence (AI) within a Geographic Information System (GIS) environment. The base principle is the ability of ML algorithms to generalize and learn from non-linear relationships, and model natural complex processes and events, which are difficult or impossible to be described with analytical mathematics (Noack, et al., 2014).

The aim of the modelling is large-scale mapping of the iron concentration and pH based on R/S multispectral data and geochemical data and elaboration of the influence of spatial and spectral resolution in the modelling process.

The accuracy and robustness of the trained network is assessed by:

- Statistical evaluation: A comparison plot of the modelling results with the measured values of iron concentration and pH.
- The network mean squared error (MSE): A converging and stable model error indicates that the network is learning effectively.
- The model distribution weights: Balanced model distribution weights indicate that the network has appropriately distributed importance across all spectral bands without overemphasizing or neglecting any specific band.
- The distribution map: Predictions should closely align with the actual target values and present uniform and logical AMD clustering.

3.2 Cross-Sensor Comparison of Sentinel-2 and Worldview-3 TOA Products

The calibration of a reliable training network requires adequate and sufficient sampling data, covering a wide range of AMD scenarios. Given the free availability of Sentinel-2 data and the typically high costs of high-resolution commercial R/S datasets, we propose a methodology where ANNs are trained using Sentinel-2 data over a large area in conjunction with extensive geochemical monitoring data. The established dependencies and relationships are then applied to commercial high-resolution datasets for targeted identification of AMD in specific areas. This approach requires that the training and application models are provided with similar controlling parameters.

Though the R/S multispectral datasets used in this study can provide “similar” observations (VNIR-SWIR for Sentinel-2 and Worldview-3 data, and VNIR for UAV data), they differ in the field of view, spatial resolution, spectral bandwidth, and spectral response function. While the difference introduced by different field of view and spatial resolution can be reduced and solved by the orthorectification and data resampling, respectively, the difference caused by different spectral bandwidth and spectral response function (the so-called reflectance difference) is a more complex problem.

In this study, we apply the linear regression approach at different wavelengths to minimize reflectance difference between two similar satellite observations over water bodies. Figure 5 shows the cross-sensor agreement analyses between the Sentinel-2 and Worldview-3 TOA data. The Sentinel-2 bands B5, B7, B8A, B11 and B12 are paired to Worldview-3, based on the introduced concept of synthesised bands by (Gasparovic, et al., 2018).

The weakest correlations are observed in the low-resolution Sentinel-2 bands, specifically B1 (443 nm), B9 (940 nm), and the blue spectral band B2 (490 nm). The low correlation in the blue wavelength range can be addressed to the fact that the reflection in this part of the spectrum is more susceptible to atmospheric scattering, which can drastically affect measurements.

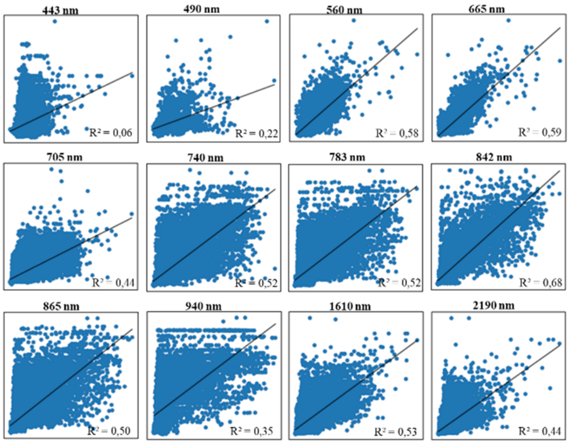

Figure 5: Cross-sensor agreement analyses between the Sentinel-2 and Worldview-3 TOA data.

Figure 6 shows examples of cross-sensor comparison of the median spectra for three lakes: Kleinleipischer See (Fe = 195 mg/L, pH = 2,56), Bergheider See (Fe = 50,2 mg/L, pH = 2,74) and Poleysee (Fe = 0,15 mg/L, pH = 3,9). In all lakes, the Sentinel-2 and Worldview-3 spectra are in good agreement in terms of shape.

Additionally, we use the transformation parameters from the linear regression model to harmonize the reflectance of Worldview-3 to Sentinel-2. The Sentinel-2 and adjusted Worldview-3 spectra are in good agreement in terms of shape and magnitude (Figure 6). However, the adjusted spectra are slightly brighter than those of Sentinel-2 within the near- and short wavelength infrared (>700-nanometers).

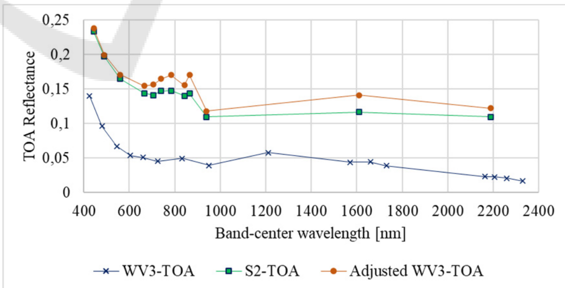

(a)

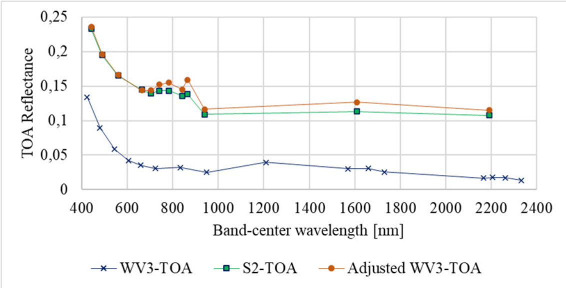

(b)

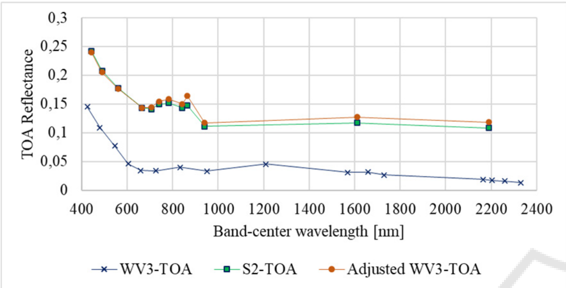

(c)

Figure 6: TOA reflectance spectra for a) Kleinleipischer See (Fe = 195 mg/L, pH = 2,56), b) Bergheider See (Fe = 50,2 mg/L, pH = 2,74) and c) Poleysee (Fe = 0,15 mg/L, pH = 3,9).

3.3 Cross-Sensor Comparison of Sentinel-2 BOA Products and UAV

Similar to section 3.2, cross-sensor agreement analyses were performed between Sentinel-2 BOA data and UAV data. The results of these analyses are presented in Figure 7. The Sentinel-2 bands B5 and B7 are paired to UAV, based on the introduced concept of synthesised bands by (Gasparovic, et al., 2018). The weakest correlations are observed in the visible part of the spectrum corresponding to Sentinel-2 B2 (490 nm), B3 (560 nm), B4 (665 nm).

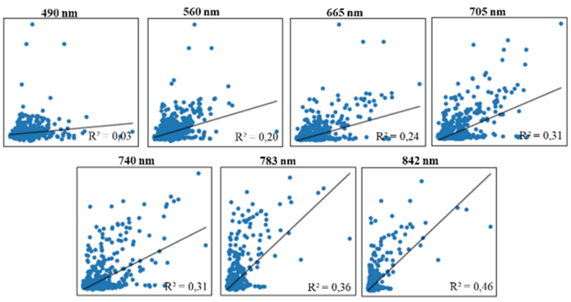

Figure 7: Cross-sensor agreement analyses between the Sentinel-2 BOA and UAV data.

A detailed view of the individual bands revealed that the visible bands are more susceptible to the ground surface brightness and reflectance differences coming from dynamically changing weather conditions.

These discrepancies are confirmed also when comparing the Sentinel-2 BOA and UAV median spectra for Scheibe See (Figure 8). Generally, both spectres in the two lakes (Bergheider and Scheibe See) are in good agreement both in terms of shape and magnitude. Due to their similarity, in this case no transformation is used to harmonize the reflectance of UAV data to Sentinel-2 BOA.

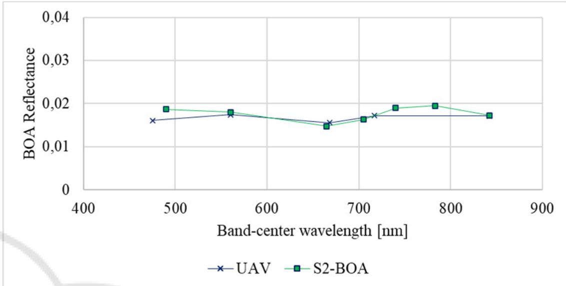

(a)

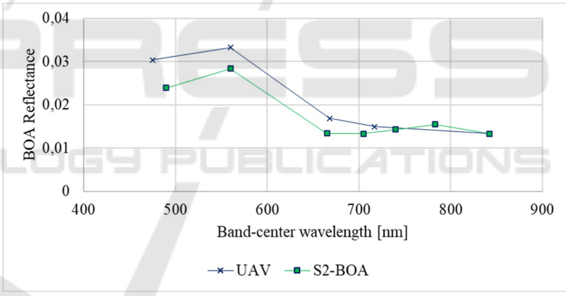

(b)

Figure 8: BOA reflectance spectra for a) Bergheider See (Fe = 50,2 mg/L, pH = 2,74), b) Scheibe See (Fe = 0,17 mg/L, pH = 7,38)

4 RESULTS

Two MLP training models were developed using Sentinel-2 and WorldView-3 data as controlling parameters. These models aim to evaluate the impact of WorldView-3's higher spatial and spectral resolution on AMD mapping. Furthermore, an application model leverages the established dependencies derived from Sentinel-2 training model and applies them to harmonized WorldView-3 data to assess the transferability of the knowledge gained in MLPs across similar remote sensing datasets.

On the other hand, the development of training models based on UAV-derived data for two lakes was deemed impractical due to the limited availability of training data. However, an application model was implemented to evaluate the transferability of the established dependencies for AMD mapping and was validated by the geochemical sampling in the two lakes.

4.1 Training Scenario Using Sentinel-2

Controlling parameters include Sentinel-2 multispectral bands of Level-1C and Level-2A products. Figure 9 shows a comparison plot of the modelling results with the measured values of iron concentration and pH values. The trained neural network has been able to reproduce the calibration data in case of the iron concentration, as an optically active parameter. In case of pH values, there are no clearly established dependencies between the controlling parameters and the calibration data, however there is a significant differentiation of the acidic from the neutral waters.

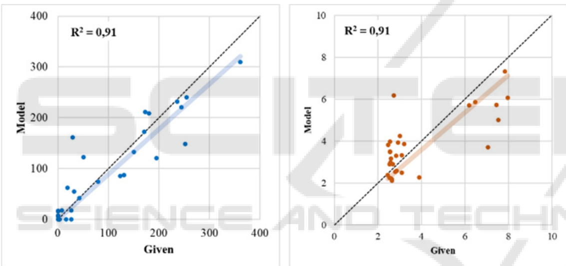

(a) (b)

Figure 9: Plot of given and modelled a) iron concentration and b) pH values based on Sentinel-2 Level-2A BOA products.

The MSE in both cases shows systematic convergence and remains stable, confirming the neural network's accuracy and robustness (Figure 10).

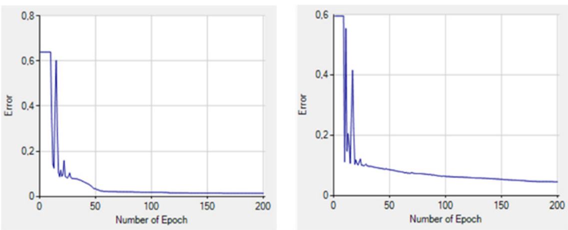

(a) (b)

Figure 10: Plot of MSE for the MLP for a) iron concentration and b) pH values based on Sentinel-2 Level-2A BOA products.

The model parameter weights revealed the Sentinel-2 Level-2A green (B03) and SWIR (B11 and B12) spectral bands to have the highest contribution for the modelling of iron concentration and B08 (NIR) and SWIR (B11 and B12) for pH values.

The result is a distribution map of iron concentration (Figure 11) and pH values (Figure 12) in the value ranges of input calibration data (0 – 361 mg/L and 2–8, respectively) over the water bodies in the AOI. The typical patterns of high iron concentrations and low pH values in the shores are mostly due to the mixed pixel information in shallow waters. Generally, the distribution map reflects the AMD severity as measured from the geochemical analysis.

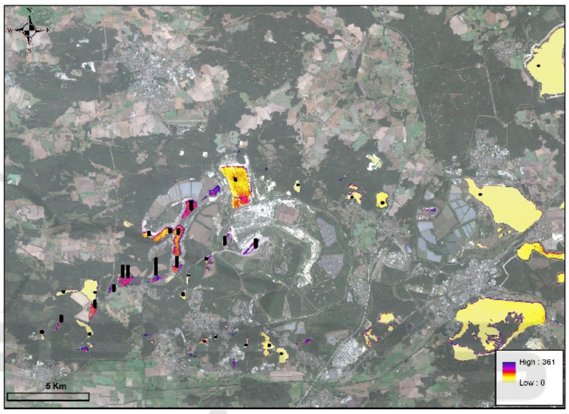

Figure 11: Distribution map of iron concentration over the water bodies in the AOI; additionally, the measured Fe values are shown as a column chart.

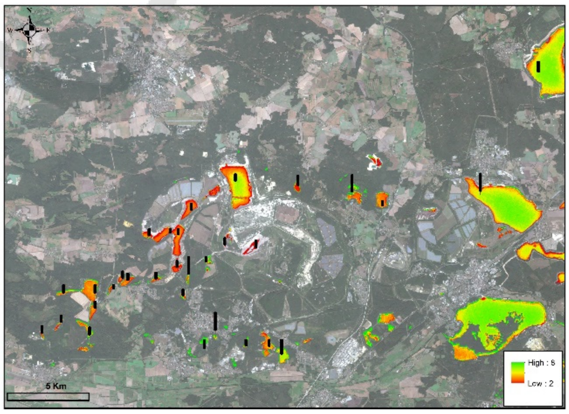

Figure 12: Distribution map of pH values over the water bodies in the AOI; additionally, the measured pH values are shown as a column chart.

4.2 Training Scenario Using Worldview-3

Controlling parameters include Worldview-3 TOA multispectral bands. In this case, the geochemical analytic results are available for about 10 post-mining water bodies in the AOI. Figure 13 shows a comparison plot of the modelling results with the measured values of iron concentration and pH values. In this case, the trained neural network has been able to better reproduce the calibration data.

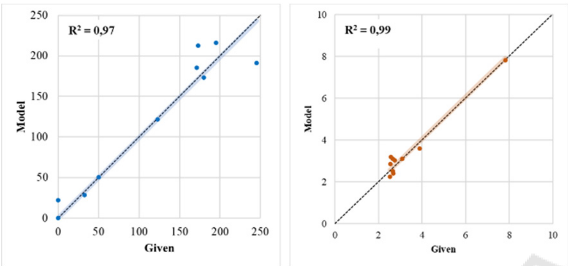

(a) (b)

Figure 13: Plot of given and modelled a) iron concentration and b) pH values based on Worldview-3 TOA products.

The MSE in both cases shows systematic convergence and remains stable, confirming the neural network's accuracy and robustness (Figure 14).

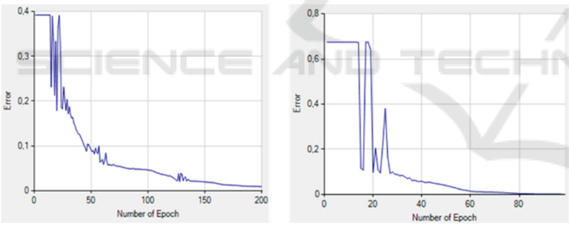

Figure 14: Plot of MSE for the MLP for a) iron concentration and b) pH values based on Worldview-3 TOA products.

Similar to the training model in 4.1, the training model weights confirmed the Worldview-3 TOA green and SWIR (from SWIR2 to SWIR7) spectral bands to have the highest contribution for the modelling of iron concentration and NIR1/2 and SWIR (SWIR6 to SWIR8) for pH values.

The resulting distribution maps of iron concentration (Figure 15) and pH values (Figure 16) reflect the AMD severity as measured from the geochemical analysis, taking into consideration only those part of the WV3-image that are free of cirrus clouds.

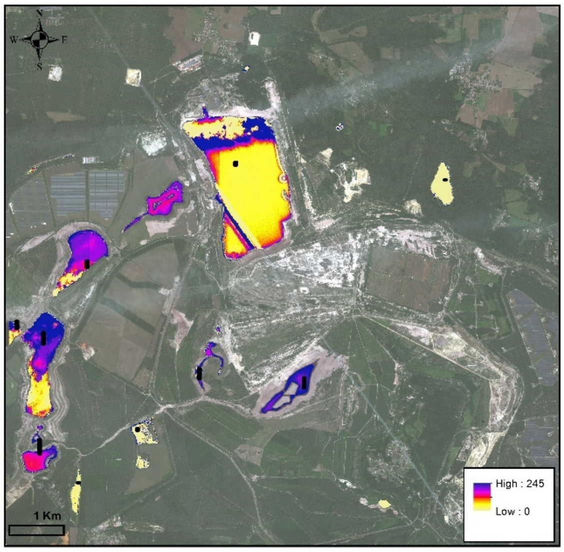

Figure 15: Distribution map of iron concentration over the water bodies in the AOI; additionally, the measured Fe values are shown as a column chart.

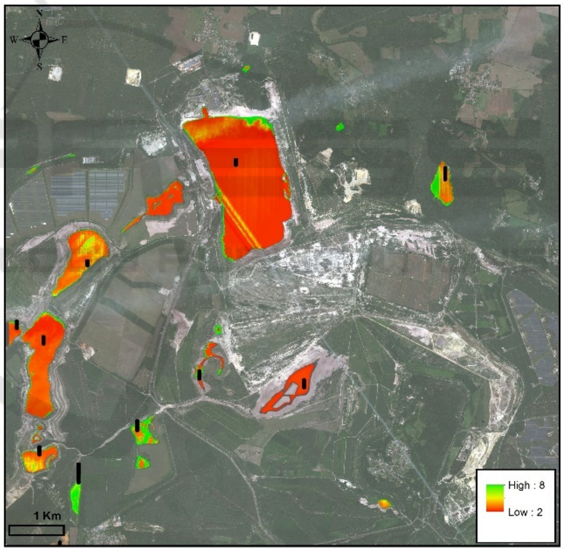

Figure 16: Distribution map of pH values over the water bodies in the AOI; additionally, the measured pH values are shown as a column chart.

4.3 Application Scenario Using Harmonized Worldview-3

This scenario is useful when there are no sufficient calibration data inside the AOI of commercial Worldview-3 data. In this case, the harmonized Worldview-3 image bands to Sentinel-2 are used as controlling parameters and the established dependencies from the training scenario in 4.1 are used for AMD mapping. This approach does not exploit the full potential of SWIR in the Worldview-3 data, since they are harmonized to SWIR bands of Sentinel-2. However, it enables AMD mapping in the shores and in small/narrow water bodies, which cannot be represented properly in medium resolution images.

Figure 17 shows a comparison plot of the application results with the measured values of iron concentration and pH values. The predicted iron concentration values resemble to the trend of measured values, but they are obviously overestimated, showing higher AMD-levels then the ones from geochemical analysis. This is reflected also in the modelled pH value, where all the water bodies in the AOI are predicted as very acidic.

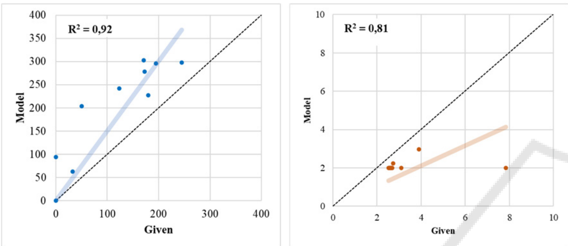

(a) (b)

Figure 17: Plot of given and modelled a) iron concentration and b) pH values based on harmonized Worldview-3 TOA products.

The same observations are confirmed from the distribution maps of iron concentration (Figure 18) and pH values (Figure 19).

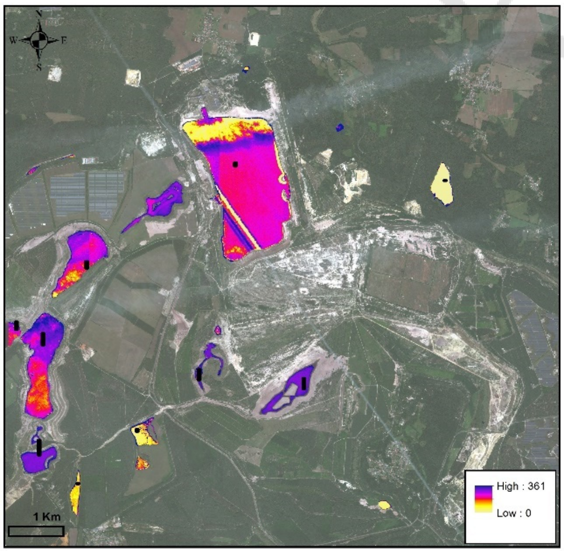

Figure 18: Distribution map of iron concentration over the water bodies in the AOI; additionally, the measured Fe values are shown as a column chart.

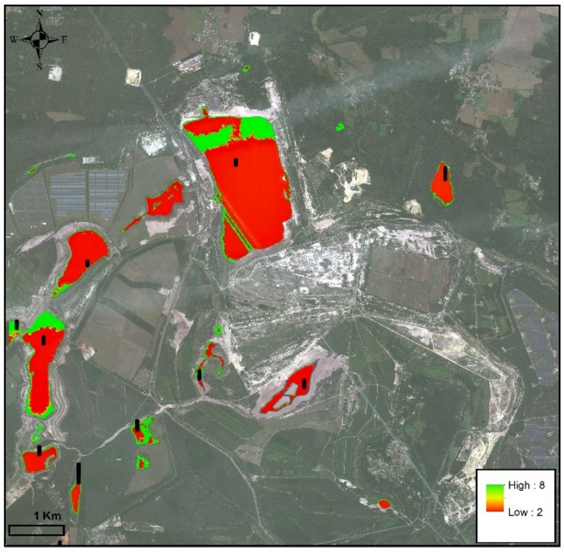

Figure 19: Distribution map of pH values over the water bodies in the AOI; additionally, the measured pH values are shown as a column chart.

4.4 Application Scenario Using UAV Data

In this scenario, a new neural network was trained by Sentinel-2 data using only bands in the VIS-VNIR. This network confirmed the Sentinel-2 Level-2A green band (B03) to have the highest contribution for modelling of iron concentration and NIR band (B08) for the pH value. The established dependencies in the trained network were used for large-scale mapping of AMD in Scheibe See and Bergheider See using UAV data.

Figure 20 and 21 show the distribution map of iron concentration and pH value over Bergheider See and Scheibe See. The median values of AMD parameters over both lakes and results of geochemical analysis are presented for comparison in Table 3.

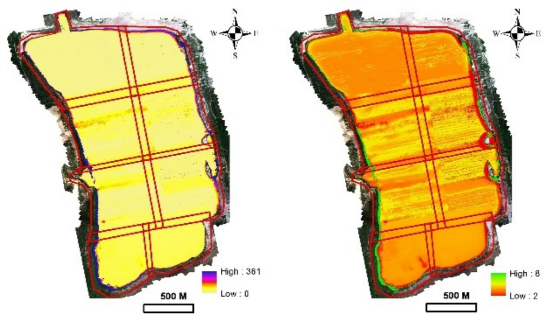

(a) (b)

Figure 20: Distribution map of a) iron concentration and b) pH value over the Bergheider See.

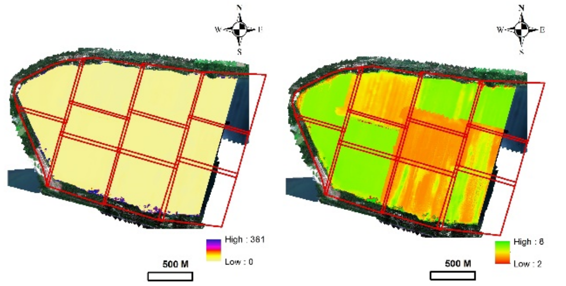

(a) (b)

Figure 21: Distribution map of a) iron concentration and b) pH value over the Scheibe See.

Table 3: Comparison of geochemistry and modelling results for Bergheider See and Scheibe See.

	Bergheider See		Scheibe See	
	Measured	Model	Measured	Model
pH	2,74	3,84	7,38	6,62[2]
Fe (mg/L)	50,2	39,3	0,17	9,4

The variating weather conditions between the mission flights seem to have a very small effect in the modelling of iron concentration, but show a considerable influence in the modelling of pH values. This issue is further elaborated in chapter 6.

5 DISCUSSION

This study assesses the feasibility of using free and commercial multispectral R/S datasets in combination with supervised ML algorithms for the automatic mapping of AMD in water bodies.

Supervised ML algorithms require large and diverse training datasets that represent a wide range of AMD scenarios. However, in practical applications, such comprehensive datasets are often unavailable. To address this limitation, the study developed training models using a large variety of water bodies exhibiting different AMD levels. The transferability of the established models was further evaluated using commercial R/S datasets.

The application of optical R/S analyses requires cloud- and cirrus-free acquisitions. Sentinel-2 data are generally more available for this purpose due to their high temporal resolution. In contrast, acquiring commercial datasets such as WorldView-3 imagery often requires careful planning, as constraints such as low cloud coverage and low nadir angles significantly influence the availability of suitable acquisitions. UAV-flight campaigns also present logistical challenges, especially for large water bodies, as they require several days of data collection under stable weather conditions to ensure consistent reflectance values across adjacent flight paths.

The high spatial and spectral resolution of WorldView-3 imagery, particularly in the SWIR bands, proved to be highly effective for AMD mapping. This may be related to the ability of SWIR bands to detect high concentrations of heavy metals typically associated with severely acidic conditions. Future research could further explore AMD patterns within the SWIR region using hyperspectral datasets, such as those provided by EnMAP or PRISMA. Additionally, the green spectral band was identified as an important feature, potentially due to the absence of vegetation or algae in water bodies with high acidity levels.

The MLP models developed in this study demonstrated robust performance but are limited by the concentration ranges defined by the calibration data. Consequently, quantitative predictions cannot be reliably extrapolated beyond the range of the calibration data. In this context, discrete sampling remains of critical importance for properly calibrating or validating the algorithms. However, the proposed approach enables large-scale AMD mapping of water bodies by significantly reducing the need on extensive sampling campaigns.

The flight campaign for a complete survey of large water bodies can take several days due to the European Union Aviation Safety Agency (EASA) restrictions for UAV (such as a maximum flight height of 120-meters). In practice, it is almost impossible to have constant weather conditions during such campaigns. The variating weather conditions (cloud, cirrus, haze, shadows) have a big influence on the surface reflectance of water bodies, leading to difficulties for balancing of the reflectance values and modelling inconsistencies over a water body.

To improve UAV-based monitoring, fixed-wing UAVs are recommended for their ability to cover larger areas efficiently, reducing weather-induced variability and resulting imbalances across flight missions. Additionally, multispectral cameras with wider spectral bands would enhance the detection of subtle water quality variations. On the other hand, increasing the UAV flight altitude would considerably reduce flight time and also improve the accuracy of photogrammetric reconstructions by enhancing feature variations between consecutive images.

[2] The median pH values for Scheibe See were derived only from tiles captured under cloudy weather conditions.

6 CONCLUSIONS

The novelty of this study is the cross-sensor comparison of free and commercial space- and airborne- multispectral R/S datasets (Sentinel-2, Worldview-3 and UAV) with a focus on assessing the transferability of established dependencies between AMD parameters and spectral data across several datasets.

The cross-sensor analysis identified spectral discrepancies coming mainly from differences in spectral bandwidth and spectral response functions. To address these variations, transformation parameters were derived to align the spectral characteristics of commercial datasets with those of Sentinel-2, which was used as a reference due to its free availability and high temporal resolution. This makes Sentinel-2 a valuable dataset for training ML algorithms.

Results indicate that adjusted WorldView-3 data appear slightly brighter than Sentinel-2 data in the NIR and SWIR (>700 nm) regions. Consequently, the transferred neural network exhibited a tendency to overestimate AMD levels. Future research can focus on optimizing transformation parameters using larger and more diverse datasets, including time-series data and broader spatial coverage. Nevertheless, the correct relative distribution of iron concentrations suggests that the established dependencies from the training model remain transferable across these datasets. This approach fully elaborates the high spatial resolution of WV3-datasets and enables AMD mapping even in small-scale or narrow water bodies, offering a more efficient and cost-effective alternative, as running extensive training models on commercial datasets.

The training scenario with the best results was obtained when using Worldview-3 datasets as controlling parameters, due to their high spatial and spectral resolution, particularly in the SWIR bands. However, the trained network in this case is relied in a few number of water bodies and AMD scenarios.

The transferred neural network for UAV-based monitoring has shown also very promising results. While clear-sky and sunny conditions offer optimal reflectance, they can introduce sun-glint effects in UAV-based monitoring. The large-scale pH distribution map of Scheibe See (Figure 21) highlighted the significant impact of weather conditions on the modelling process. In Bergheider See, flight missions occurred under more consistent conditions, resulting in minimal weather-related influences. These findings suggest that bright, diffused sunlight represents the ideal weather conditions for UAV-based water quality monitoring.

Finally, despite not being included in any training scenarios, Scheibe See was correctly classified as a lake with no evidence of AMD, demonstrating the applicability of the trained neural network beyond the AOI. This demonstrates the robustness and application of the developed approach for large-scale mapping of the water quality in post-mining water bodies.

ACKNOWLEDGEMENTS

This research has been done within the framework of the project S34I—Secure and sustainable supply of raw materials for EU industry¬, coordinated by Ana C. Teodoro. This project has received funding from the European Union’s HORIZON Research and Innovation. Grant Agreement No. 101091616 (https://doi.org/10.3030/101091616). Portuguese National Funds also support this work through the FCT – Fundação para a Ciência e a Tecnologia, I.P. (Portugal), projects UIDB/04683/2020 (https://doi.org/ 10.54499/UIDB/04683/2020) and UIDP/04683/2020 (https://doi.org/10.54499/UIDP/04683/2020).

The authors are grateful to LMBV for providing the water monitoring data, which made this research study possible. The authors gratefully acknowledge also the comments and suggestions of three anonymous reviewers, which led to a substantial improvement in the manuscript.

REFERENCES

Agisoft LLC. (n.d.). *Metashape scripts* [GitHub repository]. https://github.com/agisoft-llc/metashape-scripts

Chastain, R., Housman, I., Goldstein, J., Finco, M., Tenneson, K. (2019). Empirical cross sensor comparison of Sentinel-2A and 2B MSI, Landsat-8 OLI, and Landsat-7 ETM+ top of atmosphere spectral characteristics over the conterminous United States, Remote Sensing of Environment, Volume 221, 2019, Pages 274-285, ISSN 0034-4257, https://doi.org/10.1016/j.rse.2018.11.012.

Copernicus. (n.d.). Sentinel-2 mission. Retrieved from https://sentiwiki.copernicus.eu/web/s2-mission

European Space Agency (ESA). (n.d.). *WorldView-3 mission*. Retrieved from https://earth.esa.int/eogateway/missions/worldview-3

Farahnakian, F., Luodes, N., Karlsson, T. (2024). “A Comparative Study of Machine Learning Models for Pixel-wise Acid Mine Drainage Classification Using Sentinel-2”. IGARSS 2024 - IEEE International Geoscience and Remote. 2024.

Gasparovic, M., Medak, D., Pilaš, I., Jurjevic, L., Balenović, I. (2018). Fusion of Sentinel-2 and PlanetScope Imagery for Vegetation Detection and Monitoring. ISPRS - International Archives of the Photogrammetry, Remote Sensing and Spatial Information Sciences. XLII-1. 155-160. 10.5194/isprs-archives-XLII-1-155-2018.

Hanelli, D., Barth, A., Volkmer, G., Köhler, M. (2023). Modelling of acid mine drainage in open pit lakes using Sentinel-2 time-series: A case study from Lusatia, Germany. Minerals 2023, 13, 271. https://doi.org/10.3390/min13020271.

Haykin, S. (1998). Neural Networks: A Comprehensive Foundation. United States: Prentice Hall PTR, Upper Saddle River, NJ, United States; ISBN 978-0-13-273350-2.

Kopačková, V. (2019). “Mapping acid mine drainage (amd) and acid sulfate soils using sentinel-2 data”. IGARSS 2019 - 2019 IEEE International Geoscience and Remote Sensing Symposium, S. pp. 5682–5685.

Lausitzer und Mitteldeutsche Bergbau-Verwaltungsgesellschaft (LMBV). (n.d.). Homepage. https://www.lmbv.de/

LBA (n.d.) *Legal basis for drone operations*. Available at: https://www.lba.de/DE/Drohnen/Allgemeine_Informationen/Rechtliche_Grundlagen/Rechtliche_Grundlagen_node.html

MicaSense. (n.d.). *MicaSense image processing* [Website]. https://micasense.github.io/imageprocessing/

MicaSense. (n.d.). *Altum-PT integration guide – MicaSense knowledge base*. Retrieved from https://support.micasense.com/hc/en-us/articles/Altum-PT-Integration-Guide

MicaSense. (n.d.). *MicaSense support center*. Retrieved from https://support.micasense.com/

Noack, S., Knobloch, A., Etzold, S. H., Barth, A., Kallmeier, E. (2014). Spatial predictive mapping using artificial neural networks. The International Archives of the Photogrammetry, Remote Sensing and Spatial Information Sciences, XL–2, 79–86.

NV5 Geospatial. (n.d.). *Homepage*. https://www.nv5geospatialsoftware.com/